Electronic Supplementary Information

Experiment Section

Materials: All chemicals, including cobalt nitrate hexahydrate ($Co(NO_3)_2\ 6H_2O$), cobalt chloride ($CoCl_2\ 6H_2O$), tellurium (Te) powder, 2-methylimidazole, methanol, perchloric acid ($HClO_4$), and cerium sulfate tetrahydrate ($CeS_2O_8\ 4H_2O$) were bought from Aladdin Ltd (Shanghai, China). Nafion solution (5 wt%) was purchased from Sigma-Aldrich. The water use throughout all experiments was purified through a Millipore system. All chemicals were used of analytical grade and used as received without further purification.

Synthesis of ZIF-67 precursors: ZIF-67 precursors were prepared by reported references. Typically, 985.2 mg 2-methylimidazole and 582 mg $Co(NO_3)_2\ 6H_2O$ were dissolved in 35 ml of methanol, respectively, gently stirring for 10 min. Then the 2-methylimidazole solution was rapidly added into $Co(NO_3)_2\ 6H_2O$ solution and stirred for 15 min. The mixed solution was aged (incubated) at room temperature for 24 h. The obtained precipitates ZIF-67 were collected by centrifugation and washed with absolute ethanol for three times. Finally, the resulting product was dried at 60℃ in vacuum for further use.

Synthesis of CoTe@NC: The above synthesized ZIF-67 precursors were further annealed with Te powder under Ar atmosphere. 50 mg ZIF-67 and 100 mg Te power were separately put into two graphite boats and annealed at 680 ℃ for 60 min at a ramp rate of 2 ℃ min^{-1} to obtain CoTe@NC.

Synthesis of CoTe: To prepare CoTe, we first annealed as-prepared ZIF-67 precursors for 6 h under 500 ℃ in air atmosphere to obtain Co_3O_4. Then 50 mg Co_3O_4 and 100 mg Te power were separately put into two graphite boats and annealed at 680 ℃ for 60 min in Ar atmosphere to get the final CoTe powder.

Synthesis of NC: Firstly, a quartz boat containing ZIF-67 (200 mg) without covering was heated up to 680 ℃ under a mixed H_2/Ar flow with 5 vol% H_2 and maintained for 60 min. The product Co@NC was collected after naturally cooling. To synthesize

NC, Co@NC was etched in 1.0 M H_2SO_4 at 80 ℃ for 24 h. Then the product NC was collected by centrifugation and dried overnight.

Characterization: X-ray diffraction (XRD) data were acquired on a Shimadzu XRD-6100 diffractometer with Cu Kα radiation (40 kV, 30 mA) of wavelength 0.154 nm. Raman spectroscopy measurements were carried out on the LabRAM HR Evolution (Horiba) with an excitation wavelength of 532 nm. Scanning electron microscopy (SEM) and energy dispersive X-ray (EDX) elemental mapping images were collected on a Gemini SEM 300 scanning electron microscope (ZEISS, Germany) at an accelerating voltage of 5 kV. X-ray photoelectron spectroscopy (XPS) measurements were performed on an ESCALABMK II X-ray photoelectron spectrometer using Mg as the exciting source. Transmission electron microscopy (TEM) images were obtained from a Zeiss Libra 200FE transmission electron microscope operated at 200 kV. Absorbance data were acquired on SHIMADZU UV-2700 Ultraviolet-visible (UV-Vis) spectrophotometer.

Electrochemical measurements: The ink was prepared by mixing 2 mg of CoTe@NC catalyst, 770 μL of isopropyl alcohol, 200 μL of H_2O, and 30 μL of Nafion and ultra-sonicating for 1 h. Then, 5 μL catalyst ink was loaded onto a pre-polished glassy carbon electrode of a rotation ring disk electrode (RRDE) (ring area: 0.1866 cm^2, disk area: 0.2475 cm^2) to achieve a catalyst loading ≈ 0.04 mg cm^{-2}. All electrochemical tests were carried on CHI 760E (CHI Instruments Inc.). The formation of H_2O_2 enabled by the active catalysts was studied by using rotating ring disk electrode (RRDE) measurements with a three-electrode system. The RRDE loaded electrocatalyst was used as the working electrode, a platinum foil as the counter electrode, and Ag/AgCl (saturation KCl) as the reference electrode. The electrolyte was 0.1 M $HClO_4$ with a pH value of 1. Note that the recorded current density was normalized to the geometric surface area. Before the linear sweep voltammetry (LSV) tests, cyclic voltammetry (CV) was performed in the potential range from 0 to 0.8 V vs. reversible hydrogen electrode (RHE) in Ar-saturated 0.1 M $HClO_4$ electrolyte at 100 mV s^{-1} for around 50 cycles. The electrochemical cleaning

of the Pt ring was then conducted in the same potential range at 200 mV s^{-1} for 20 cycles. The collection efficiency is determined as 35%. Electrochemical impedance spectroscopy (EIS) was conducted at 0.3 V vs. RHE from 100 KHz to 0.1 Hz. The H_2O_2 production performances (activity and selectivity) were assessed by LSV scans (scan rate: 5 mV s^{-1}, RRDE rotating speed: 1,600 rpm) in the potential range of 0.0 to 0.8 V vs. RHE. During the LSV tests, the applied potential to the Pt was held at 1.2 V vs. RHE for H_2O_2 detection.

The H_2O_2 selectivity (H_2O_2(%)), and electron transfer number (n) were calculated as follows:

$$H_2O_2\ (\%) = 200 \times (I_{Ring}/N)/(I_{Disk} + I_{Ring}/N) \quad (1)$$

$$n = 4|I_{Disk}|/(I_{Disk} + I_{Ring}/N) \quad (2)$$

Where I_{Ring} is the ring current, I_{Disk} is the disk current.

H_2O_2 produced via bulk ORR electrolysis can be accumulated and quantified during the bulk ORR electrolysis in 0.1 M $HClO_4$. The direct electrosynthesis of H_2O_2 and quantification of H_2O_2 concentration were carried out in a gas-tight H-cell system. The CoTe@NC (loading 0.1 mg) on a carbon paper electrode (0.5 cm × 0.5 cm) was prepared as the cathode electrode (CoTe@NC/CP). A Nafion 117 membrane was employed to separate the chambers. The membrane was protonated by first treating in H_2O_2 aqueous solution (5 wt.%) at 80 ℃ for 1 h, then washed with deionized water until the pH value of the water returned to normal. Finally, the membranes were soaked with deionized water for 4 h. The electrochemical experiments were carried out with a CHI 760E using a three-electrode configuration with prepared CoTe@NC/CP electrode, Pt mesh electrode, and Ag/AgCl electrode as the working electrode, the counter electrode, and the reference electrode, respectively.

Cobalt leaching phenomenon of CoTe@NC and CoTe during the long-term stability tests were measured by inductively coupled plasma mass spectrometry (ICP-MS) using a Shimadzu ICPMS-2030 spectrometer. ICP-MS standard solutions were prepared by dissolving $CoCl_2$ $6H_2O$ in a solution of 0.1 M $HClO_4$.

Quantitative detection of H_2O_2: H_2O_2 yield was measured by using the indicator of

$Ce(SO_4)_2$ ($2Ce^{4+} + H_2O_2 \rightarrow 2Ce^{3+} + 2H^+ + O_2$). Samples (20 μL tested electrolyte) were collected at a certain time (1 h) and mixed with the $Ce(SO_4)_2$ solution (0.1 mmol L^{-1}, 3.98 mL). The generated solution was detected with a UV-Vis spectrophotometer. A typical concentration-absorbance curve was calibrated by linear fitting the absorbance values at wavelength length of 320 nm for various known concentrations of 0, 0.02, 0.04, 0.06, 0.08, and 0.1 mM of Ce^{4+}. The yield of H_2O_2 was finally determined based on the reduced Ce^{4+} concentration.

The density functional theory (DFT) calculation details: First-principles calculations with spin-polarized were performed based on density functional theory (DFT) implemented in the VASP package,[1] and the interaction between valence electrons and ionic core were expanded using the projector augmented wave (PAW)[2] approach with a cutoff of 500 eV. Perdew-Burke-Ernzerhof functional (PBE) with semi-empirical corrections of DFT-D3 was adopted to describe exchange-correlation functional effect[3] based on general gradient approximation (GGA). We modeled the catalyst using CoTe (101) and (102) surface with six layers, for which the middle two layers were fixed to mimic the bulk. The thickness of the vacuum region is >15 Å to avoid the spurious interaction. The Brillouin zone were sampled by $4 \times 6 \times 1$ and $3 \times 6 \times 1$ special k-points using the Monkhorst Pack scheme for structural configuration optimizations of CoTe (101) and (102), respectively.[4] The force convergence thresholds are 0.02 eV/Å and the total energy less than 1E-5 eV, respectively.

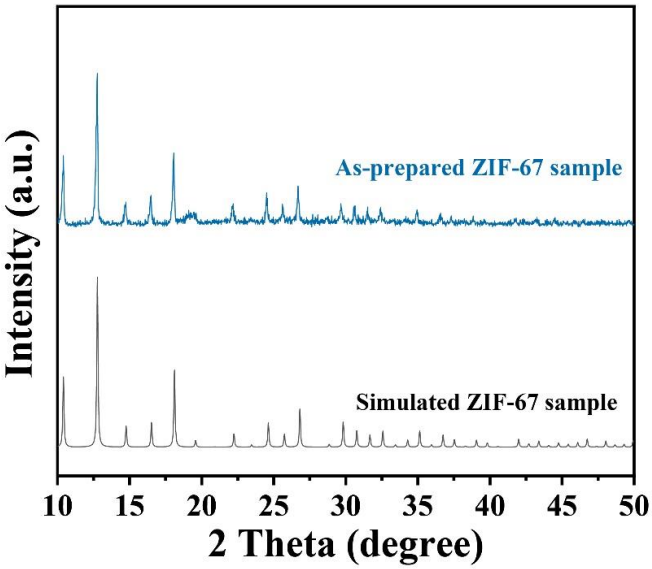

Fig. S1 XRD pattern of as-prepared ZIF-67.

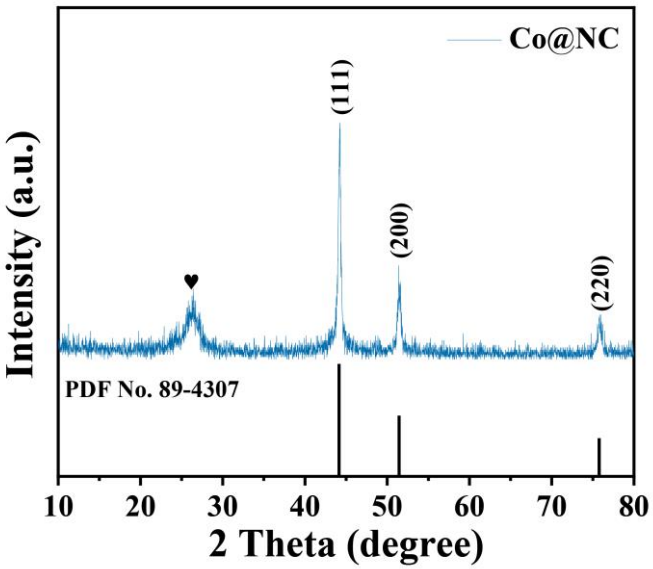

Fig. S2 XRD pattern of Co@NC.

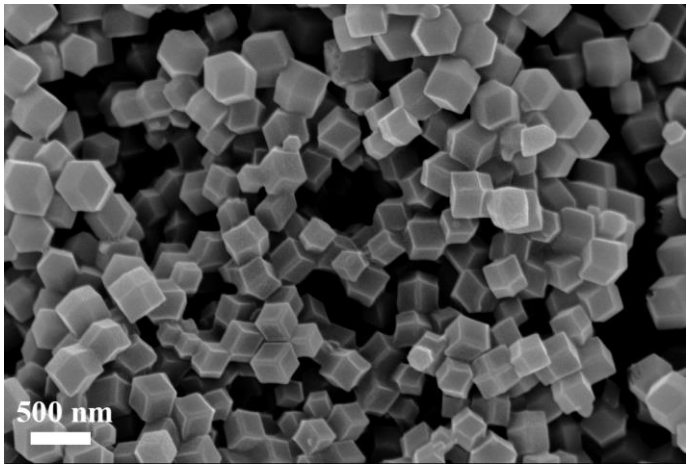

Fig. S3 SEM image for ZIF-67.

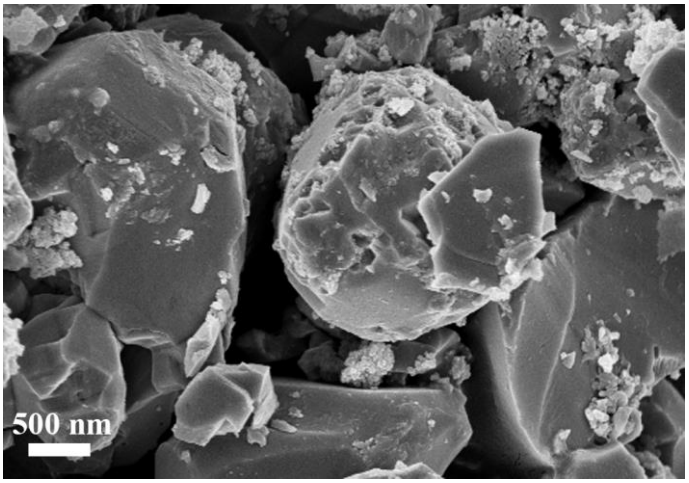

Fig. S4 SEM image for pure CoTe.

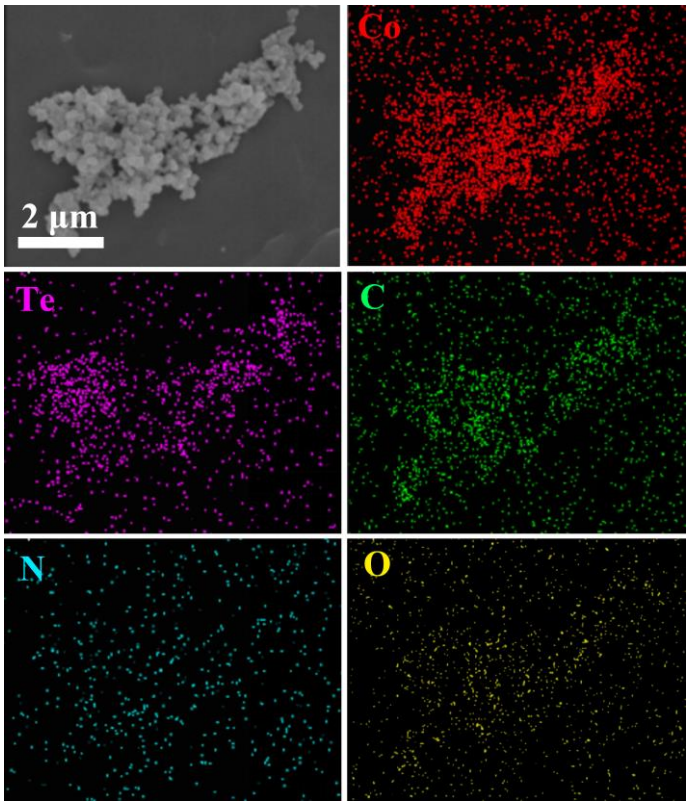

Fig. S5 SEM and EDX elemental mapping images of Co, Te, C, N, and O for CoTe@NC.

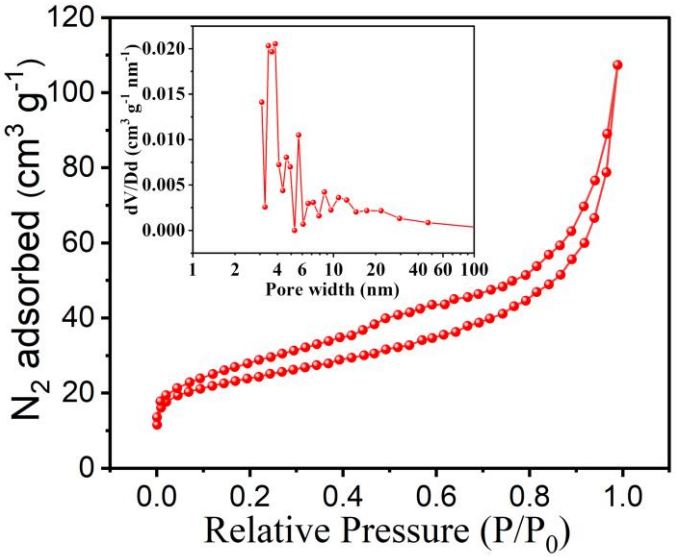

Fig. S6 N_2 adsorption-desorption isotherms and the corresponding pore size distribution (inset) of CoTe@NC.

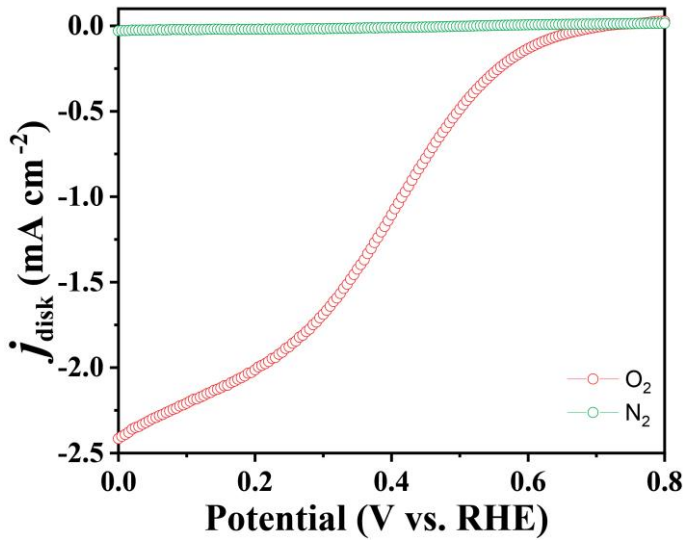

Fig. S7 RRDE voltammograms of CoTe@NC at 1600 rpm in O_2- and N_2-saturated 0.1 M $HClO_4$.

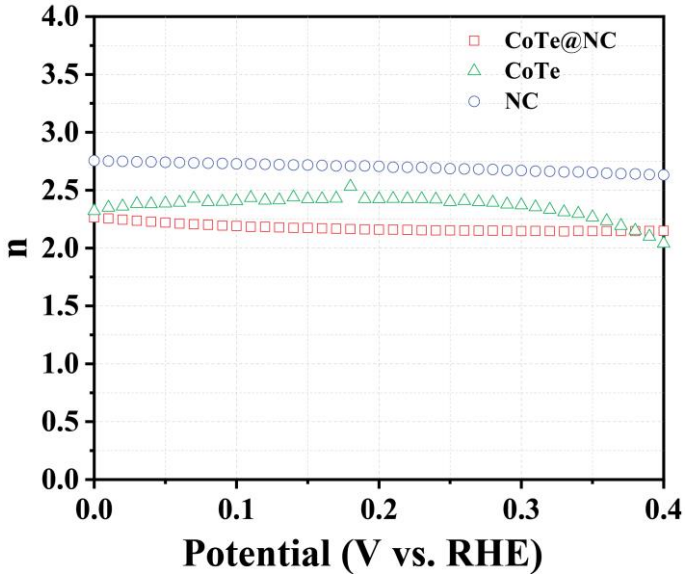

Fig. S8 Calculated electron transfer number (n) as a function of applied potential for CoTe@NC, CoTe, and NC.

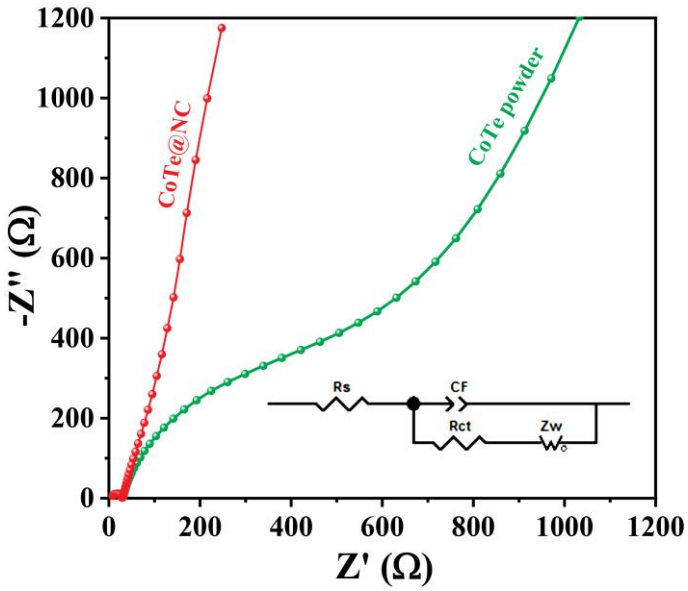

Fig. S9 Nyquist plots of CoTe@NC and CoTe in O_2 saturated 0.1 M $HClO_4$ solution.

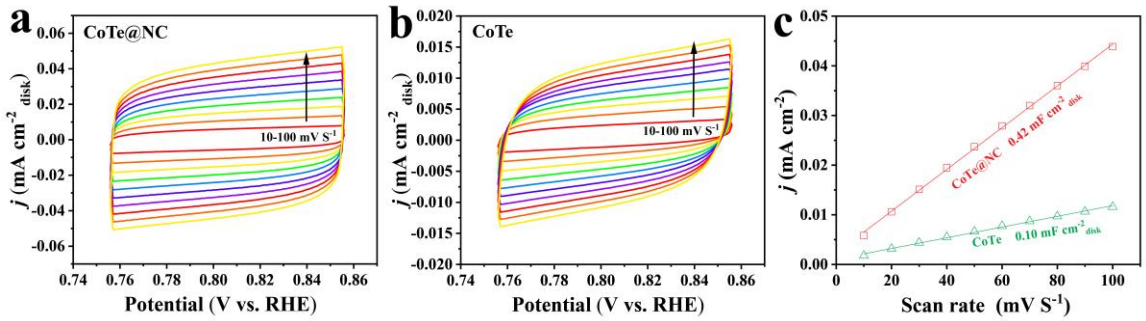

Fig. S10 Cyclic voltammograms for (a) CoTe@NC and (b) CoTe in the double layer region at scan rates of 10, 20, 30, 40, 50, 60, 70, 80, 90, and 100 mV s^{-1} in 0.1 M $HClO_4$. (c) Capacitive currents as a function of scan rate at 0.806 V of CoTe@NC and CoTe.

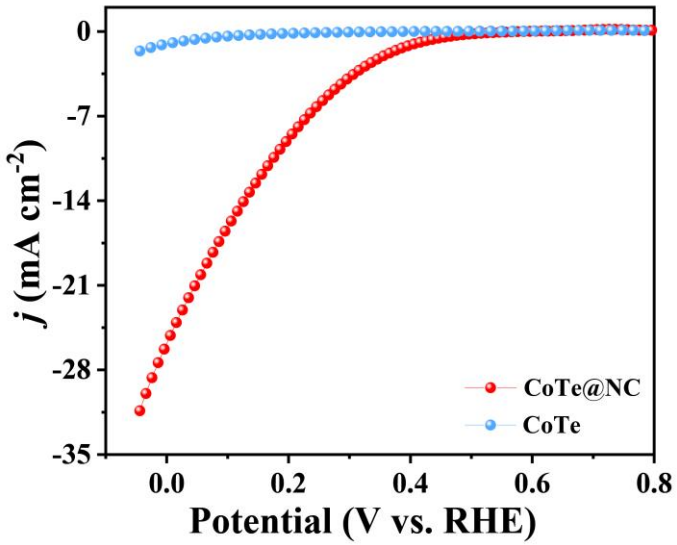

Fig. S11 LSV curves for CoTe@NC and CoTe in the H-cell tests.

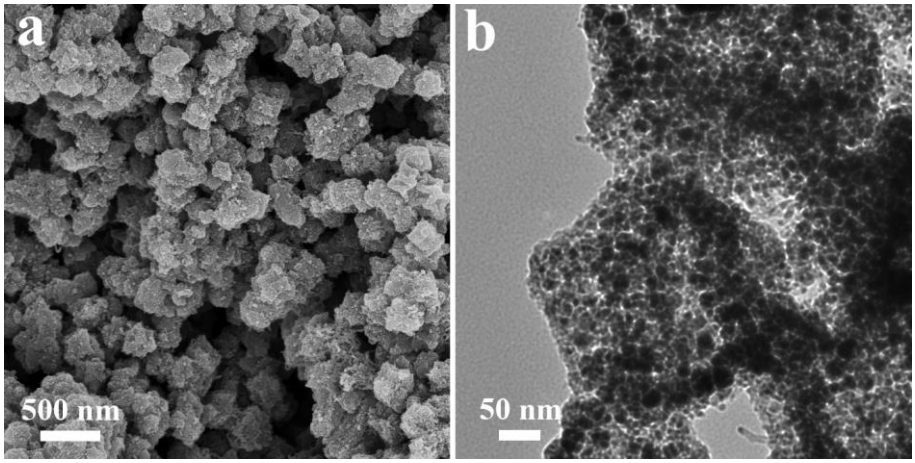

Fig. S12 (a) SEM image and TEM image for post-ORR CoTe@NC.

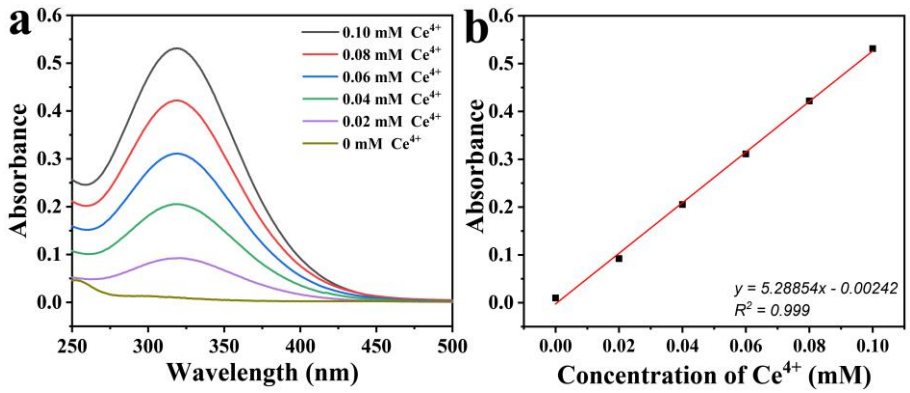

Fig. S13 (a) UV-Vis spectra of Ce^{4+} solution with various concentrations and (b) corresponding standard curve.

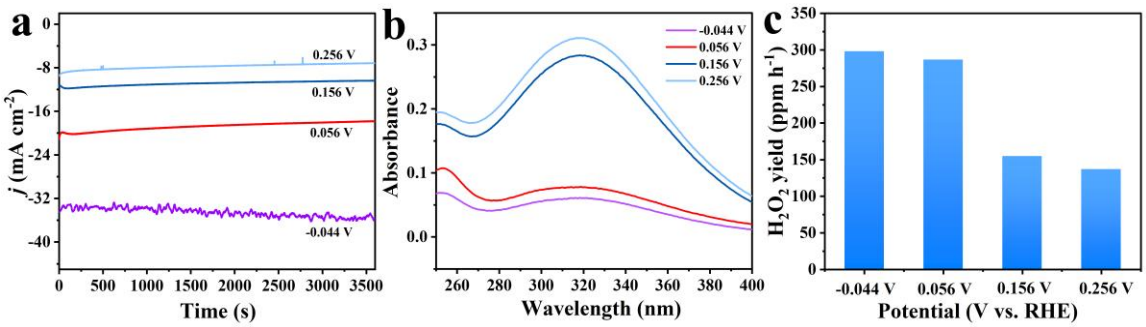

Fig. S14 (a) Chronoamperometry curves for CoTe@NC under various potentials for 3600 s. Corresponding (b) UV-Vis spectra and (c) H_2O_2 yields in an H-type cell.

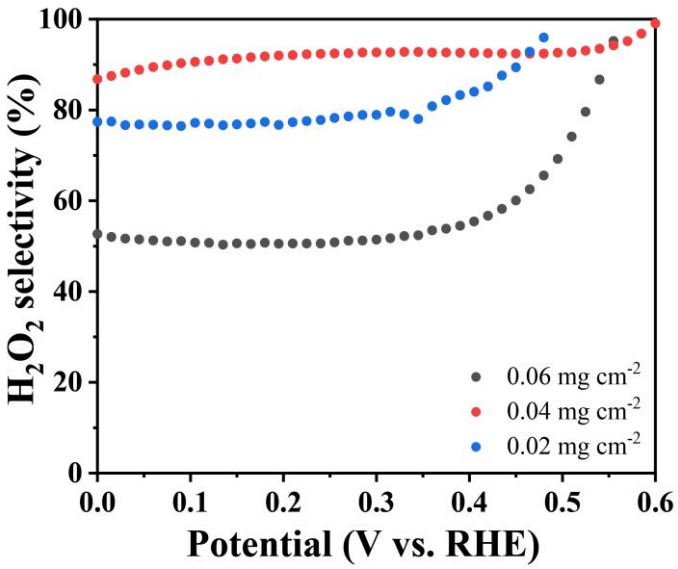

Fig. S15 H_2O_2 selectivity of CoTe@NC at different loadings (0.02 mg cm^{-2}, 0.04 mg cm^{-2}, and 0.06 mg cm^{-2}).

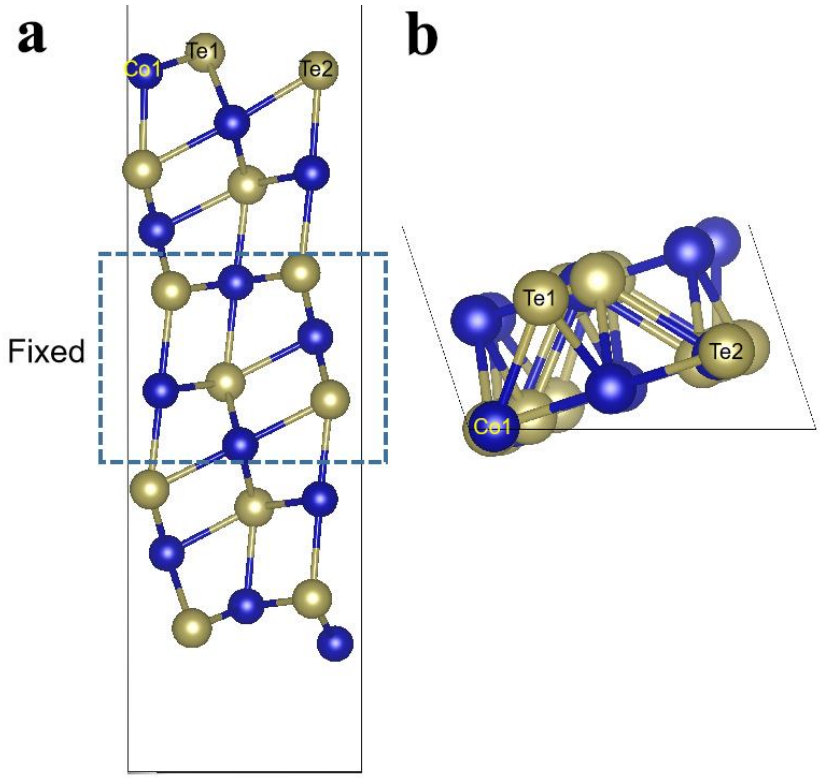

Fig. S16 (a) Side and (b) top views of the CoTe (101) surface, in which the middle two layers (enclosed with the dashed lines) are fixed to mimic the bulk. The considered adsorption sites (Co1, Te1 and Te2) for the OOH species are marked in both (a) and (b).

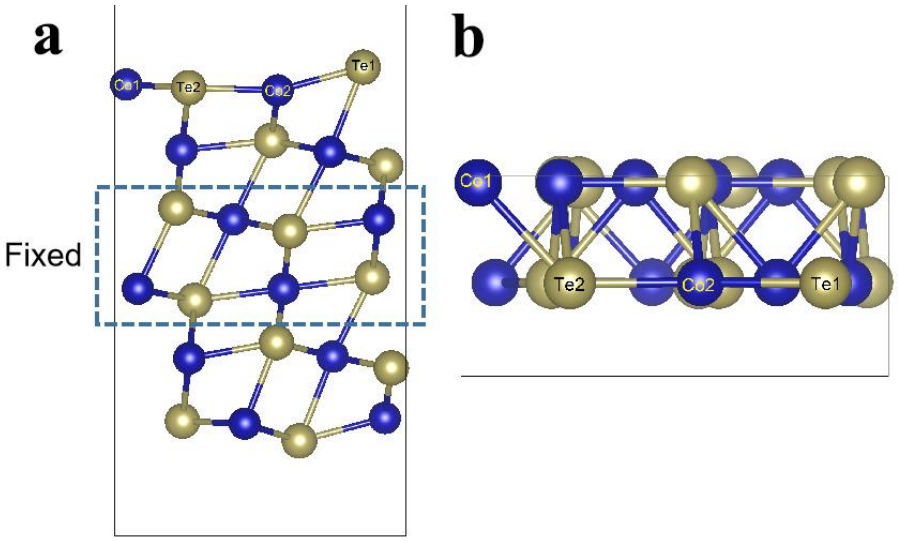

Fig. S17 (a) Side and (b) top views of the CoTe (102) surface, in which the middle two layers (enclosed with the dashed lines) are fixed to mimic the bulk. The considered adsorption sites (Co1, Co2, Te1 and Te2) for the OOH species are marked in both (a) and (b).

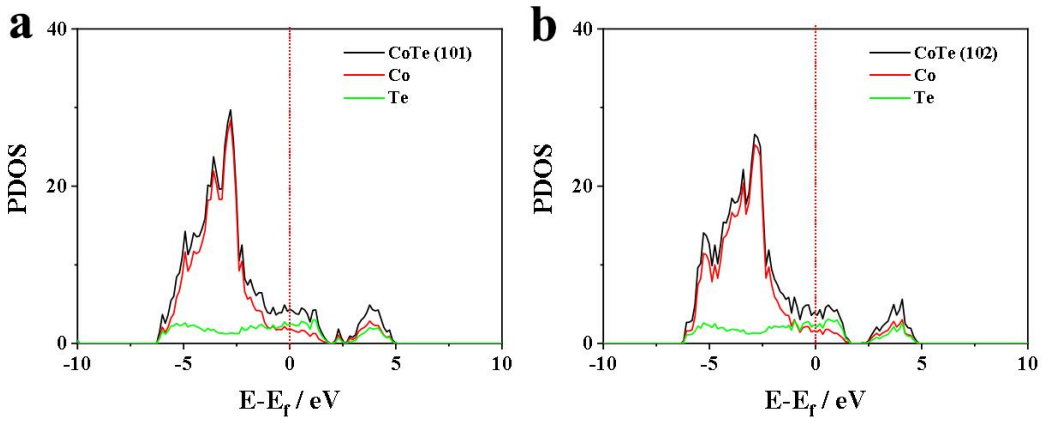

Fig. S18 Projected density of states of the (a) CoTe (101) and (b) CoTe (102) surface.

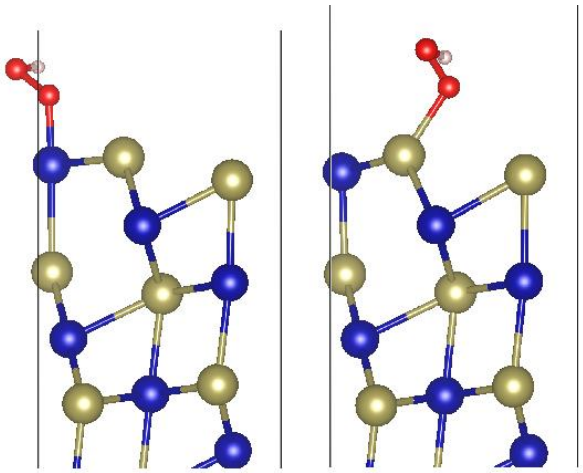

(101)

Fig. S19 Side view of the adsorbed OOH at the Co1 and Te1 sites for CoTe (101).

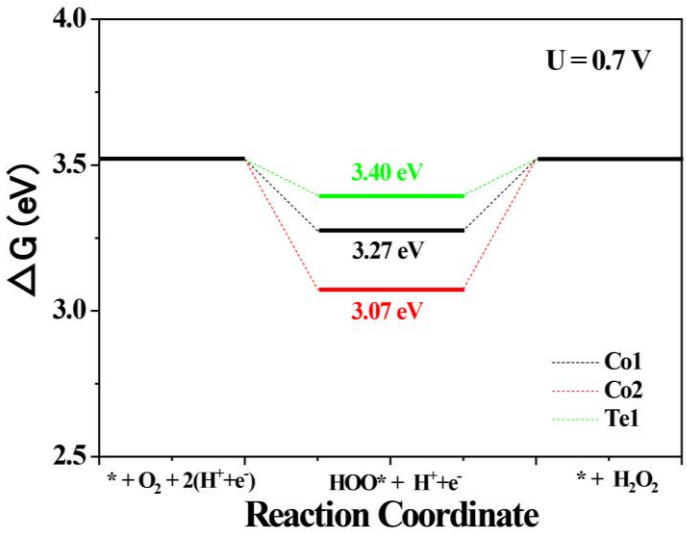

Fig. S20 Free energy diagrams of oxygen reduction to H_2O_2 on the CoTe (102) at U = 0.7 V, the inset is side view of the adsorbed OOH at the Te1 site.

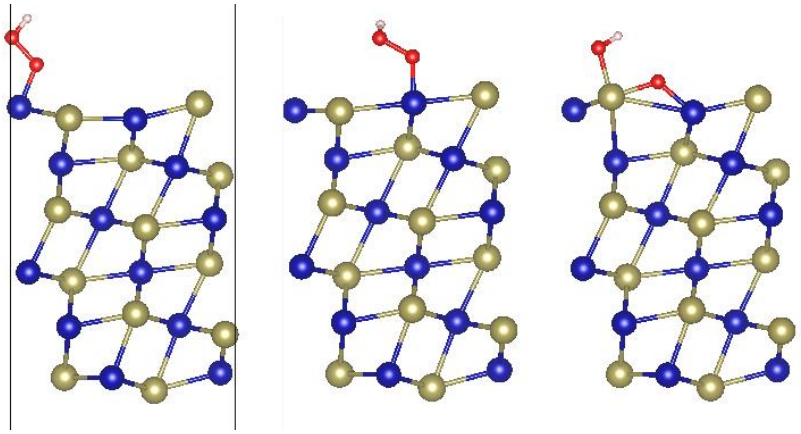

Fig. S21 Side view of the adsorbed OOH at the Co1, Co2 and Te2 sites for CoTe (102).

Table S1 Comparison of CoTe@NC with recent 2e$^-$ ORR electrocatalysts for H_2O_2 production in acidic media.

Catalyst	Selectivity (%@V vs. RHE)	Overpotential (V vs. RHE)	Electrolyte	Accumulation (mg L^{-1} @V vs. RHE)	Stability	Catalyst loading (mg cm^{-2})	Ref.
CoTe@NC	**92.6@0.3**	**0.004**	**0.1 M $HClO_4$**	**277.3@0.056 V (60 min)**	**12 h (H-cell)**	**0.04**	**This work**
Pt-Hg NPs/C	90@0.4	0.1	0.1 M $HClO_4$	N/A	8000 cycles	N/A	[5]
Pt/HSC	94@0.5	0.1	0.1 M $HClO_4$	2.64@0V (60 min)	6 h	0.05	[6]
C(Pt)/C	41@0.1	0	1 M $HClO_4$	N/A	24 h	0.08	[7]
Pt/TiN	55@0.33	0.05	0.1 M $HClO_4$	N/A	1h	0.175	[8]
Pt/TiC	68@0.2	0.25	0.1 M $HClO_4$	N/A	1000 cycles	0.0225	[9]
$CoSe_2$@NCNTs	93.2@0.3	0.005	0.1 M $HClO_4$	172@0 V (60 min)	24 h	0.05	[10]
h-Pt_1-CuS_x	92@0.05	0.05	0.1 M $HClO_4$	546 ±30 mol kg_{cat}^{-1} (60 min)	10000 cycles	0.101	[11]
Au/C	80@0.1	N/A	0.1 M $HClO_4$	N/A	N/A	N/A	[12]
$Au_{0.92}Pd_{0.08}$/C	95@0	0.04	0.1 M $HClO_4$	N/A	N/A	0.11	[13]
FPC-800	80@0.1	0.27	0.05 M H_2SO_4	112.6 mmol g^{-1} (60 min)	24 h	0.202	[14]
g-N-CNHs	90@0.2	0.295	0.1 M H_2SO_4	54 mmol g^{-1} h^{-1} cm^{-2}	6 h	0.07	[15]
meso-BMP	20@0.1	0.07	0.1 M $HClO_4$	5@0.1 V (60 min)	N/A	0.307	[16]
meos-BMP-800	65.2@0.1	0.12	0.1 M $HClO_4$	0.26 (60 min)	5.74 h	0.325	[17]
RF-AQ-XC72	83@0	0.44	0.5 M H_2SO_4	18@0.1 V (60 min)	N/A	2.5	[18]
FePc/C	78.2@-0.24	N/A	0.1 M H_2SO_4 and 0.1 M K_2SO_4	160@–1 V (60 min)	N/A	N/A	[19]
O-CNTs	52@0.1	0.4	0.1 M $HClO_4$	N/A	N/A	0.1	[20]
PtP_2 NCs	90@0.35	0.005	0.1 M $HClO_4$	2.26 mmol cm^{-2} (60 min)	N/A	N/A	[21]
PEI50CMK3-800T	95@0.05	0.245	0.5 M H_2SO_4	N/A	N/A	0.05	[22]
Co/carbon	80@0.4	0.08	0.5 M H_2SO_4	5 μmmol cm^{-2} (60 min)	N/A	1	[23]
Mn-O/N@NCs	74@0.2	0.005	0.1 M $HClO_4$	N/A	N/A	N/A	[24]
Co-N-C	75@0.3	N/A	0.5 M H_2SO_4	N/A	N/A	0.1	[25]
Co_1-NG(O)	43@0.55	0.005	0.1M $HClO_4$	N/A	N/A	0.01	[26]
CoN@CNTs	90@0.3	0.02	0.1 M $HClO_4$	633.25@0.3 V (60 min)	12 h	0.25	[27]
CoS_2	70@0.5	0.15	0.05 M H_2SO_4	148@0.5 V (60 min)	N/A	0.305	[28]
$CoSe_2$	70@0.45	0.05	0.05 M H_2SO_4	91.16@0.5V (60 min)	4 h	0.305	[29]
$MoTe_2$/Graphene	90@0.3	0.14	0.5 M H_2SO_4	N/A	5000 cycles	0.01	[30]
{001}-Fe_2O_{3-x}	91@0.3	0.14	0.005 M H_2SO_4	N/A	N/A	3.0	[31]

Table S2 ICP-MS analysis of 0.1 M $HClO_4$ after the bulk electrolysis runs for CoTe@NC and CoTe.

ICP-MS sample		Intensity	Standard Curve	[Co] in Diluted ICP-MS Sample	Average [Co] in electrolyte	Average Cobalt Leaching Rate
Standard solution of Co^{2+}	[Co] = 0 ug_{Co} L^{-1}	473.34	y = 18154.99 x - 1549.2 (R^2 = 0.9997)	/	/	/
	[Co] = 5 ug_{Co} L^{-1}	86938.60		/	/	/
	[Co] = 10 ug_{Co} L^{-1}	182849.63		/	/	/
	[Co] = 20 ug_{Co} L^{-1}	361608.87		/	/	/
	[Co] = 30 ug_{Co} L^{-1}	541900.25		/	/	/
	[Co] = 40 ug_{Co} L^{-1}	715661.58		/	/	/
	[Co] = 50 ug_{Co} L^{-1}	913747.99		/	/	/
CoTe@NC		298587.92	/	$Label_1$= 17.05 ug_{Co} L^{-1} $Label_2$= 16.26 ug_{Co} L^{-1} $Label_3$= 16.09 ug_{Co} L^{-1}	83.25 ug_{Co} L^{-1}	2.91 μg_{Co} h^{-1}
CoTe		46436646.38	/	$Label_1$= 2576.29 ug_{Co} L^{-1} $Label_2$= 2559.78 ug_{Co} L^{-1} $Label_3$= 2561.26 ug_{Co} L^{-1}	12828.9 ug_{Co} L^{-1}	449.01 μg_{Co} h^{-1}

References

1 G. Kresse and J. Hafner, *Phys. Rev. B Condens Matter.*, 1994, **49**, 14251-14269.

2 G. Kresse and D. Joubert, *Phys. Rev. B*, 1999, **59**, 1758-1775.

3 J. P. Perdew, K. Burke and M. Ernzerhof, *Phys. Rev. Lett.*, 1996, **77**, 3865-3868.

4 H. J. Monkhorst and J. D. Pack, *Phys. Rev. B*, 1976, **13**, 5188-5192.

5 S. Siahrostami, A. Verdaguer-Casadevall, M. Karamad, D. Deiana, P. Malacrida, B. Wickman, M. Escudero-Escribano, E. A. Paoli, R. Frydendal, T. W. Hansen, I. Chorkendorff, I. E. Stephens and J. Rossmeisl, *Nat. Mater.*, 2013, **12**, 1137-1143.

6 C. H. Choi, M. Kim, H. C. Kwon, S. J. Cho, S. Yun, H. T. Kim, K. J. Mayrhofer, H. Kim and M. Choi, *Nat. Commun.*, 2016, **7**, 10922.

7 C. H. Choi, H. C. Kwon, S. Yook, H. Shin, H. Kim and M. Choi, *J. Phys. Chem. C*, 2014, **118**, 30063-30070.

8 S. Yang, J. Kim, Y. J. Tak, A. Soon and H. Lee, *Angew. Chem. Int. Ed.*, 2016, **55**, 2058-2062.

9 S. Yang, Y. J. Tak, J. Kim, A. Soon and H. Lee, *ACS Catal.*, 2017, **7**, 1301-1307.

10 L. Zhang, J. Liang, L. Yue, Z. Xu, K. Dong, Q. Liu, Y. Luo, T. Li, X. Cheng, G. Cui, B. Tang, A. A. Alshehri, K. A. Alzahrani, X. Guo and X. Sun, *Nano Res.*, 2021, DOI: 10.1007/s12274-021-3474-0.

11 R. Shen, W. Chen, Q. Peng, S. Lu, L. Zheng, X. Cao, Y. Wang, W. Zhu, J. Zhang, Z. Zhuang, C. Chen, D. Wang and Y. Li, *Chem*, 2019, **5**, 2099-2110.

12 J. S. Jirkovsky, M. Halasa and D. J. Schiffrin, *Phys. Chem. Chem. Phys.*, 2010, **12**, 8042-8052.

13 J. S. Jirkovsky, I. Panas, E. Ahlberg, M. Halasa, S. Romani and D. J. Schiffrin, *J. Am. Chem. Soc.*, 2011, **133**, 19432-19441.

14 K. Zhao, Y. Su, X. Quan, Y. Liu, S. Chen and H. Yu, *J. Catal.*, 2018, **357**, 118-126.

15 D. Iglesias, A. Giuliani, M. Melchionna, S. Marchesan, A. Criado, L. Nasi, M. Bevilacqua, C. Tavagnacco, F. Vizza, M. Prato and P. Fornasiero, *Chem*, 2018, **4**, 106-123.

16 F. Haschè, M. Oezaslan, P. Strasser and T.-P. Fellinger, *J. Energy Chem.*, 2016, **25**, 251-257.

17 T. P. Fellinger, F. Hasche, P. Strasser and M. Antonietti, *J. Am. Chem. Soc.*, 2012, **134**, 4072-4075.

18 A. Wang, A. Bonakdarpour, D. P. Wilkinson and E. Gyenge, *Electrochim. Acta*, 2012, **66**, 222-229.

19 F. L. Silva, R. M. Reis, W. R. P. Barros, R. S. Rocha and M. R. V. Lanza, *J. Electroanal.Chem.*, 2014, **722-723**, 32-37.

20 Z. Lu, G. Chen, S. Siahrostami, Z. Chen, K. Liu, J. Xie, L. Liao, T. Wu, D. Lin, Y. Liu, T. F. Jaramillo, J. K. Nørskov and Y. Cui, *Nat. Catal.*, 2018, **1**, 156-162.

21 H. Li, P. Wen, D. S. Itanze, Z. D. Hood, S. Adhikari, C. Lu, X. Ma, C. Dun, L. Jiang, D. L. Carroll, Y. Qiu and S. M. Geyer, *Nat. Commun.*, 2020, **11**, 3928.

22 Y. Sun, S. Li, Z. P. Jovanov, D. Bernsmeier, H. Wang, B. Paul, X. Wang, S. Kuhl and P. Strasser, *ChemSusChem*, 2018, **11**, 3388-3395.

23 A. Bonakdarpour, D. Esau, H. Cheng, A. Wang, E. Gyenge and D. P. Wilkinson, *Electrochim. Acta*, 2011, **56**, 9074-9081.

24 A. Byeon, J. Cho, J. M. Kim, K. H. Chae, H. Y. Park, S. W. Hong, H. C. Ham, S. W. Lee, K. R. Yoon and J. Y. Kim, *Nanoscale Horiz.*, 2020, **5**, 832-838.

25 Y. Sun, L. Silvioli, N. R. Sahraie, W. Ju, J. Li, A. Zitolo, S. Li, A. Bagger, L. Arnarson, X. Wang, T. Moeller, D. Bernsmeier, J. Rossmeisl, F. Jaouen and P. Strasser, *J. Am. Chem. Soc.*, 2019, **141**, 12372-12381.

26 E. Jung, H. Shin, B. H. Lee, V. Efremov, S. Lee, H. S. Lee, J. Kim, W. H. Antink, S. Park, K. S. Lee, S. P. Cho, J. S. Yoo, Y. E. Sung and T. Hyeon, *Nat. Mater.*, 2020, **19**, 436-442.

27 Q. Zhang, X. Tan, N. M. Bedford, Z. Han, L. Thomsen, S. Smith, R. Amal and X. Lu, *Nat. Commun.*, 2020, **11**, 4181.

28 H. Sheng, E. D. Hermes, X. Yang, D. Ying, A. N. Janes, W. Li, J. R. Schmidt and S. Jin, *ACS Catal.*, 2019, **9**, 8433-8442.

29 H. Sheng, A. N. Janes, R. D. Ross, D. Kaiman, J. Huang, B. Song, J. R. Schmidt and S. Jin, *Energy Environ. Sci.*, 2020, **13**, 4189-4203.

30 X. Zhao, Y. Wang, Y. Da, X. Wang, T. Wang, M. Xu, X. He, W. Zhou, Y. Li, J. N. Coleman and Y. Li, *Natl. Sci. Rev.*, 2020, **7**, 1360-1366.

31 R. Gao, L. Pan, Z. Li, C. Shi, Y. Yao, X. Zhang and J. J. Zou, *Adv. Funct. Mater.*, 2020, **30**, 1910539.